

CLCN2 chloride channel mutations in familial hyperaldosteronism type II

Ute I. Scholl^{1,2*}, Gabriel Stölting^{3,18}, Julia Schewe^{1,18}, Anne Thiel¹, Hua Tan³, Carol Nelson-Williams^{4,5}, Alfred A. Vichot^{4,5}, Sheng Chih Jin⁴, Erin Loring^{4,5,6}, Verena Untiet³, Taekyeong Yoo⁷, Jungmin Choi^{4,5}, Shengxin Xu⁸, Aihua Wu⁸, Marieluise Kirchner⁹, Philipp Mertins⁹, Lars C. Rump¹, Ali Mirza Onder¹⁰, Cory Gamble¹¹, Daniel McKenney¹², Robert W. Lash¹³, Deborah P. Jones¹⁴, Gary Chune¹⁵, Priscila Gagliardi¹⁶, Murim Choi⁷, Richard Gordon⁸, Michael Stowasser⁸, Christoph Fahlke³ and Richard P. Lifton^{4,5,6,17}

Primary aldosteronism, a common cause of severe hypertension¹, features constitutive production of the adrenal steroid aldosterone. We analyzed a multiplex family with familial hyperaldosteronism type II (FH-II)² and 80 additional probands with unsolved early-onset primary aldosteronism. Eight probands had novel heterozygous variants in *CLCN2*, including two de novo mutations and four independent occurrences of a mutation encoding an identical p.Arg172Gln substitution; all relatives with early-onset primary aldosteronism carried the *CLCN2* variant found in the proband. *CLCN2* encodes a voltage-gated chloride channel expressed in adrenal glomerulosa that opens at hyperpolarized membrane potentials. Channel opening depolarizes glomerulosa cells and induces expression of aldosterone synthase, the rate-limiting enzyme for aldosterone biosynthesis. Mutant channels show gain of function, with higher open probabilities at the glomerulosa resting potential. These findings for the first time demonstrate a role of anion channels in glomerulosa membrane potential determination, aldosterone production and hypertension. They establish the cause of a substantial fraction of early-onset primary aldosteronism.

More than 1.1 billion people worldwide have hypertension³, the single largest cause of premature mortality⁴. About 6% of hypertensive patients in primary care have primary aldosteronism¹, with higher frequencies among patients with severe hypertension. The plasma aldosterone level in primary aldosteronism is constitutively elevated despite low levels of the normal upstream regulator renin; hypokalemia is variable. Aldosterone-producing adrenal adenomas (APAs) and idiopathic hyperaldosteronism⁵ are common causes of primary aldosteronism. Somatic mutations in *KCNJ5*, *CACNA1D*, *ATP1A1* or *ATP2B3* that cause increased glomerulosa cell Ca²⁺

are sufficient for producing APAs^{6–10}; germline mutations alter *CYP11B2*¹¹ in glucocorticoid-remediable aldosteronism (GRA, also known as FH-I), *KCNJ5*^{6,12} in FH-III, *CACNA1H*¹³ in FH-IV and *CACNA1D*⁷ in PASNA syndrome¹⁴. These mutations define a common pathway for induction of aldosterone biosynthesis—glomerulosa cell membrane depolarization activates voltage-gated Ca²⁺ channels, which induces the rate-limiting enzyme for aldosterone biosynthesis, aldosterone synthase (encoded by *CYP11B2*), along with other enzymes in the biosynthetic pathway; increased mitochondrial Ca²⁺ may also contribute¹⁵.

In 1992, Stowasser et al. described a multiplex kindred featuring autosomal dominant primary aldosteronism that was clinically distinct from GRA, the only dominant syndrome then known, and hence called it FH-II². The responsible gene in this kindred has not been identified. We recruited an additional affected individual of this kindred^{2,16} (family 3; Fig. 1, Table 1 and Supplementary Note) and performed exome sequencing¹³ of three affected subjects, identifying two shared novel protein-changing heterozygous variants in *CLCN2* (chr. 3: g.184075850C>T (hg19), p.Arg172Gln, NP_004357) and *LINGO1* (chr. 15: g.77906476G>C, p.His591Gln, NP_116197) (Supplementary Table 1). *CLCN2* was considered the more likely candidate gene on the basis of conservation (Fig. 1), expression levels in human adrenal cortex (8.14 for *CLCN2*, 5.91 for *LINGO1*, log₂ scale, mean expression of all genes = 7.20⁶) and segregation analysis in the pedigree (Fig. 1 and Supplementary Table 2).

We next searched for rare (allele frequency <10⁻⁵ in public databases) damaging¹⁷ variants in *CLCN2* and *LINGO1* among the exomes of 35 unrelated individuals diagnosed with unsolved primary aldosteronism by age 10 years—an extreme phenotype¹³. Only *CLCN2* showed such variants. All four were heterozygous and were absent in public databases (Supplementary Table 1). Notably, one

¹Department of Nephrology, Medical School, Heinrich Heine University Düsseldorf, Düsseldorf, Germany. ²Department of Nephrology and Medical Intensive Care, Charité-Universitätsmedizin Berlin, Berlin Institute of Health, Berlin, Germany. ³Institute of Complex Systems, Zelluläre Biophysik (ICS-4), Forschungszentrum Jülich, Jülich, Germany. ⁴Department of Genetics, Yale University School of Medicine, New Haven, CT, USA. ⁵Howard Hughes Medical Institute, Yale University School of Medicine, New Haven, CT, USA. ⁶Yale Center for Mendelian Genomics, New Haven, CT, USA. ⁷Department of Biomedical Sciences, Seoul National University College of Medicine, Seoul, Republic of Korea. ⁸Endocrine Hypertension Research Center, University of Queensland Diamantina Institute, Greenslopes and Princess Alexandra Hospitals, Brisbane, Queensland, Australia. ⁹Proteomics Platform, Max Delbrück Center for Molecular Medicine in the Helmholtz Society and Core Unit of Proteomics, Berlin Institute of Health, Berlin, Germany. ¹⁰Nephrology, Le Bonheur Children's Hospital, Memphis, TN, USA. ¹¹Cooper Clinic, PA, Fort Smith, AR, USA. ¹²Peyton Manning Children's Hospital at St. Vincent, Indianapolis, IN, USA. ¹³Division of Metabolism, Endocrinology and Diabetes, University of Michigan Medical School, Ann Arbor, MI, USA. ¹⁴Division of Nephrology and Hypertension, Department of Pediatrics, Vanderbilt University School of Medicine, Nashville, TN, USA. ¹⁵Olin Teague Veterans Administration Hospital, Temple, TX, USA. ¹⁶Division of Endocrinology, Nemours Children's Specialty Care, Jacksonville, FL, USA. ¹⁷Laboratory of Human Genetics and Genomics, The Rockefeller University, New York, NY, USA. ¹⁸These authors contributed equally: Gabriel Stölting and Julia Schewe. *e-mail: ute.scholl@charite.de

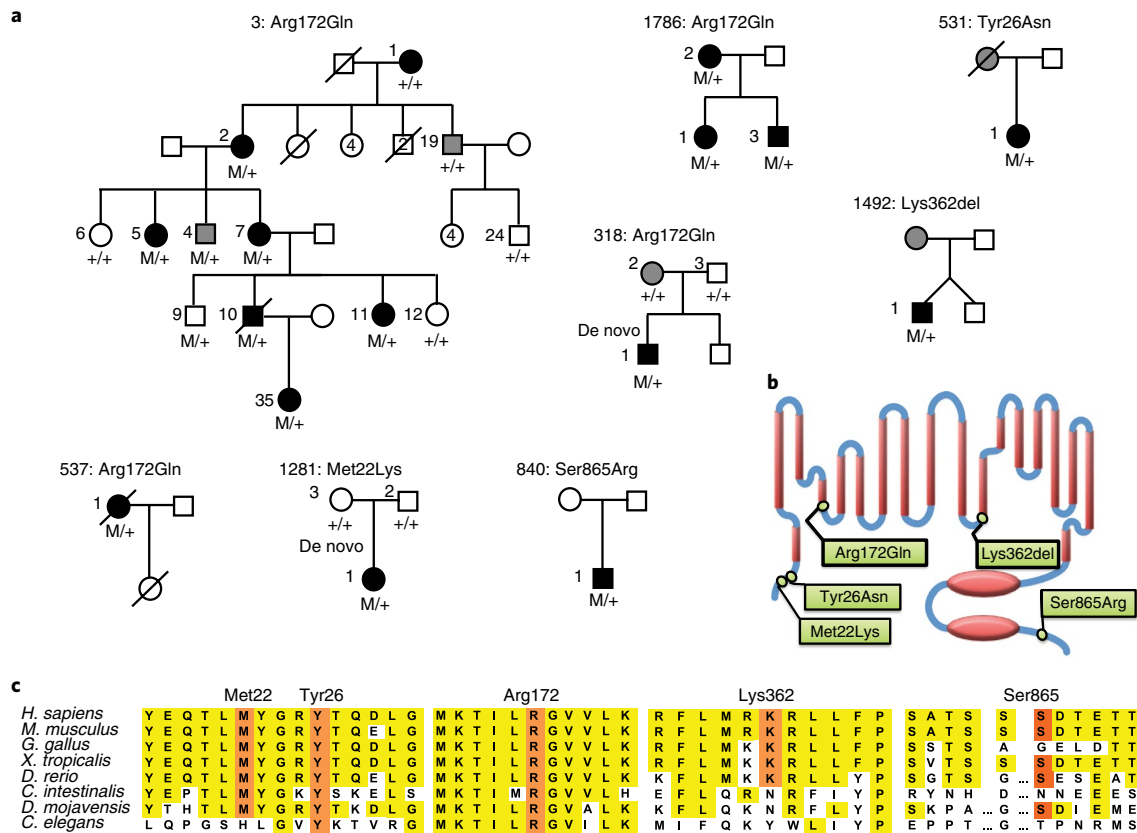


Fig. 1 | Kindreds with hypertension and primary aldosteronism with *CLCN2* mutations. a, Pedigrees of eight kindreds with primary aldosteronism and hypertension, with the indicated novel *CLCN2* variants. Filled black symbols denote subjects with primary aldosteronism, and filled gray symbols denote subjects with early-onset hypertension or borderline elevated ARR. Genotypes are shown beneath each symbol: M/+ denotes the indicated novel *CLCN2* variant in the heterozygous state and +/+ denotes homozygous wild-type sequence. **b**, Position of the indicated variants in the N terminus, D helix, K helix and C terminus of the CIC-2 chloride channel encoded by *CLCN2*. Red ellipses represent C-terminal CBS domains. **c**, Conservation of the respective amino acid positions among orthologous species (*H. sapiens*, human; *M. musculus*, mouse; *G. gallus*, chicken; *X. tropicalis*, western clawed frog; *D. rerio*, zebrafish; *C. intestinalis*, vase tunicate; *D. mojavensis*, fruit fly; *C. elegans*, roundworm). Conserved surrounding amino acid positions are shown in yellow, and conservation of the mutated residue is shown in orange.

proband had the identical p.Arg172Gln variant found in family 3. In the three additional subjects, chr. 3: g.184076918A>T (p.Met22Lys) and chr. 3: g.184076907A>T (p.Tyr26Asn) occurred at positions conserved from invertebrates to humans and one variant produced a new splice donor site resulting in an in-frame deletion (chr. 3: g.184074782T>A, p.Lys362del) (Fig. 1).

Analysis of *CLCN2* in 45 additional unrelated subjects diagnosed with primary aldosteronism by age 20 years (Supplementary Table 3) identified two further occurrences of p.Arg172Gln (Fig. 1). Additionally, chr. 3: g.184064498T>G (p.Ser865Arg) occurred at a moderately conserved position (Fig. 1). Sanger sequencing confirmed all variants (Supplementary Fig. 1). Sequencing of the Arg172 codon in 1,587 additional subjects referred for potential Mendelian hypertension, including 375 with primary aldosteronism diagnosed after age 20 years, identified no p.Arg172Gln variants, supporting enrichment of this variant in early-onset primary aldosteronism.

Among the four kindreds with p.Arg172Gln, the mutation was de novo in one kindred (kindred 318; absent in the proband's biological parents; Fig. 1 and Supplementary Table 4). Among the other three kindreds, the maximum lengths of shared mutation-linked haplotypes between pairs of individuals ranged from 4,894 to 357,885 bp (Supplementary Table 5), with the putative last shared ancestor occurring ~651 (95% confidence interval (CI), 203–2,615) to ~50,000 (95% CI, 10,000–infinity) generations ago¹⁸. Although

extremely remote common ancestry is a possibility, independent occurrence is overwhelmingly likely. After finding this mutation in the first family, the probability of finding, by chance, three additional independent instances of the mutation encoding p.Arg172Gln (one de novo) among 80 probands is 6.5×10^{-12} (Methods). The probability of any pair of these mutations being identical by descent from a remote common ancestor is even lower. Lastly, the burden of rare protein-altering *CLCN2* variants in primary aldosteronism kindreds is significantly higher than in controls (8/81 versus 6/3,578, $P = 1.3 \times 10^{-10}$, relative risk = 58.9; Supplementary Table 6).

Sanger sequencing identified eight carriers of the p.Arg172Gln variant in family 3 (Fig. 1, Table 1, Supplementary Fig. 1 and Supplementary Note). Seven carriers had an elevated aldosterone/renin ratio (ARR; a screening test for primary aldosteronism); those tested had positive confirmatory fludrocortisone suppression tests (FSTs) and non-lateralizing aldosterone production. One subject had repeatedly normal ARR, suggesting incomplete penetrance. Subject 3-1, diagnosed with hypertension in her thirties and with primary aldosteronism at age 66 years, was wild type for *CLCN2* (Supplementary Table 2). In addition to having later onset, she was distinct in having increased aldosterone with upright posture, typical of sporadic idiopathic hyperaldosteronism⁷. In kindred 1786, the proband's affected mother and brother carried the p.Arg172Gln variant. The brother had borderline ARR with suppressed renin and prehypertension at age 13 years. Subject 1492-1 was diagnosed with

Table 1 | Clinical characteristics of subjects with *CLCN2* variants

Family ID	Subject ID	<i>CLCN2</i> variant	Sex	Age dx or blood draw (years)	BP (mm Hg)	BP %ile	K ⁺ (mM)	Aldo (ng/dl)	PRA (ng/ml/h)	ARR (ng/dl:ng/ml/h)
Normal range					<140/90 in adults	<95th in children	3.5–5.5			<20
3	2	p.Arg172Gln	F	24	120/80 on 3 meds	NA	3.0	40.2	0.3	134.0
3	4	p.Arg172Gln	M	36	98/70 (age 24)	NA	4.2	24.5	1.2	20.4
3	5	p.Arg172Gln	F	19	150/100 on 1 med	NA	3.3	27.4	0.1	274.0
3	7	p.Arg172Gln	F	20	140/100	NA	3.8	26.5	0.1	265.0
3	9	p.Arg172Gln	M	18	120/80 (age 19)	NA	4.0	24.7	1.5	16.5
3	10	p.Arg172Gln	M	17	130/85	90–95th	4.0	26.2	0.1	262.0
3	11	p.Arg172Gln	F	14	94/62	≤50th	4.0	21.2	0.1	212.0
3	35	p.Arg172Gln	F	16	170/110	>99th	3.4	25.5	≤0.2	≥127.5
1786	1	p.Arg172Gln	F	15	150/100	>99th	2.9	47.9	<1.0	>47.9
1786	2	p.Arg172Gln	F	32	118/68 on 2 meds	NA	3.0	46.3	<1.0	>46.3
1786	3	p.Arg172Gln	M	13	121/75 (24 h)	>75th	4.4	12.0	<0.6	>20.0
537	1	p.Arg172Gln	F	11	160/120	>99th	3.0	26.0	0.3	86.7
318	1	p.Arg172Gln	M	7	170/140	>99th	2.6	9.5	0.21	45.2
1281	1	p.Met22Lys	F	1	117/71	>99th	4.1	17.0	<0.5	>34.0
531	1	p.Tyr26Asn	F	6	280/188 at age 20	NA	NA	100.0	<3.0	>33.3
840	1	p.Ser865Arg	M	15	130/100	90–95th/>99th	3.2	37.0	0.2	185.0
1492	1	p.Lys362del	M	0.2	150/90	>99th	4.0	63.8	<0.15	>425.3

Age dx, age at diagnosis; BP, blood pressure (office unless otherwise indicated); BP %ile, blood pressure percentile for subjects under age 18 years; K⁺, serum potassium level; Aldo, serum aldosterone level; PRA, plasma renin activity; ARR, aldosterone/renin ratio; F, female; M, male; NA, not available or not applicable; med(s), antihypertensive medication(s). Reference values are given below each parameter heading.

hypertension and primary aldosteronism in infancy but became normotensive by age 2, suggesting variable expressivity with age. Among other probands, the mutation encoding the p.Met22Lys variant was de novo (Supplementary Table 4). Thus, in two of the four kindreds with parental data, the rare *CLCN2* mutations were de novo.

In silico splice-site analysis¹⁹ of the variant in kindred 1492 predicted the creation of a new splice donor site at the end of exon 10, 3 bp upstream of the normal splice donor site. In a splicing assay in HEK cells (Supplementary Note), the wild-type exon was normally spliced but the mutation resulted exclusively in splicing at the predicted upstream site, producing an in-frame deletion of codon 362 (Supplementary Fig. 1).

CIC-2, the chloride channel encoded by *CLCN2*, is found in many tissues, including brain, kidney, lung and intestine²⁰. Additionally, *CLCN2* RNA is found in the adrenal gland. Immunohistochemistry with an antibody specific for CIC-2 showed intense staining of human adrenal zona glomerulosa (Fig. 2 and Supplementary Fig. 2), consistent with a role in regulating aldosterone production.

Chloride channels can conduct excitatory (membrane-depolarizing) chloride efflux or inhibitory influx, depending on the chloride gradient across the cell membrane. We determined the intracellular chloride concentration ($[Cl^-]_{int}$) in mouse adrenal gland slices (Fig. 3a,b and Supplementary Fig. 2) using fluorescence lifetime imaging microscopy (FLIM); the method is based on the concentration-dependent fluorescence quenching of a chloride-sensitive dye²¹. The median value of $[Cl^-]_{int}$ was 74.7 mM. The distribution of intracellular glomerulosa chloride concentrations was rather broad, as expected for a dynamic equilibrium in cells with oscillating membrane potentials²². With a normal plasma Cl⁻ concentration of 100 mM, the calculated chloride reversal potential at 37 °C is –8 mV, predicting that opening of CIC-2 in glomerulosa cells will result in chloride efflux and depolarization from the resting potential

of about –80 mV²². This depolarization is predicted to activate voltage-gated Ca²⁺ channels, inducing aldosterone biosynthesis.

A facultative subunit of CIC-2 in glia, GlialCAM, also known as HEPACAM²³, is not expressed in human adrenal gland (Genotype-Tissue Expression (GTEx) portal; see URLs). We therefore expressed wild-type CIC-2 (CIC-2^{WT}) and each of the mutant CIC-2 proteins (CIC-2^{MUT}) alone in HEK293T cells and performed whole-cell patch-clamp electrophysiology at $[Cl^-]_{int} = 75$ mM. CIC-2^{WT} channels are closed at depolarized voltages and activate slowly at voltages negative to the chloride reversal potential^{20,24,25}. All mutants shifted the activation curve to more positive voltages (Fig. 3, Supplementary Fig. 3 and Supplementary Table 8). CIC channels are homodimers, with each subunit forming a separate pore. Each of these conduction pathways can be individually opened and closed by a fast protopore gate, while a common slow gating mechanism acts on both pores^{24,26}. Whereas p.Ser865Arg slowed down deactivation of both gates and altered the protopore open probability, all other variants modified the common gate by increasing its minimum open probability and accelerating its activation (Fig. 3 and Supplementary Fig. 3). Mass spectrometry demonstrated that Ser865 was phosphorylated, suggesting a regulatory mechanism (Supplementary Fig. 4). The observed gating alterations with the CIC-2^{MUT} channels predict significantly larger chloride efflux versus CIC-2^{WT} channels in glomerulosa cells at physiological membrane potentials.

To characterize the impact of the CIC-2^{WT} and CIC-2^{MUT} channels in human adrenal glomerulosa cells, we expressed these channels in human H295R adrenocortical cancer cells, an established model of aldosterone production²⁷. Confocal microscopy showed partial colocalization of YFP-tagged CIC-2^{WT} and CIC-2^{MUT} with a cell surface membrane marker; the Met22Lys variant showed less colocalization than CIC-2^{WT} (Supplementary Fig. 4). RNA-seq (Fig. 4a and Supplementary Table 9) demonstrated that transfection

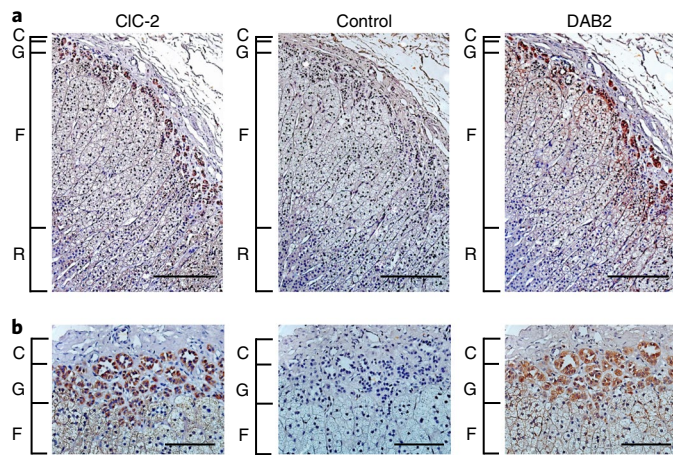


Fig. 2 | Expression of CIC-2 in human adrenal gland. **a**, Sections of human adrenal cortex (C, capsule; G, glomerulosa; F, fasciculata; R, reticularis) stained by immunohistochemistry and counterstained with hematoxylin. One of two technical replicates is shown. Left, anti-CIC-2 antibody; middle, control in which the anti-CIC-2 antibody was preincubated with the antigenic peptide; right, anti-DAB2 antibody for a marker of the adrenal zona glomerulosa. Comparison of the three panels demonstrates specific expression of CIC-2, predominantly in the zona glomerulosa. Scale bars, 200 μm . **b**, Sections of the zona glomerulosa at higher magnification. Scale bars, 100 μm .

of cells to express untagged wild-type or Arg172Gln CIC-2 in both cases significantly increased expression of *CYP11B2* and its upstream regulator *NR4A2* (*NURR1*)²⁸; *RGS4*, which provides feedback inhibition of angiotensin II (Ang II)-triggered signaling²⁹, was also upregulated. Quantitative real-time PCR of *CYP11B2* showed that transfection with *CLCN2*^{MUT} produced significantly greater increases in *CYP11B2* expression than were observed with *CLCN2*^{WT} (Fig. 4b). In contrast, transfection with *CLCN2* encoding loss-of-function mutations³⁰ did not change *CYP11B2* expression (Supplementary Fig. 5). H295R cells and their subclone HAC15 have negative membrane potentials³¹. Current-clamp recordings demonstrated significant depolarization of HAC15 cells upon expression of wild-type CIC-2; the p.Arg172Gln substitution amplified this effect (Fig. 4c).

The finding of four independent occurrences of p.Arg172Gln (one de novo), along with four additional novel variants (one de novo), among 81 probands with early-onset primary aldosteronism provides strong evidence implicating these variants in disease pathogenesis. The localization of CIC-2 in adrenal zona glomerulosa is consistent with this observation. The electrophysiological impact of mutant channels and their effects on aldosterone synthase expression demonstrate that the corresponding mutations cause gain of function, producing membrane depolarization and increasing *CYP11B2* expression (Fig. 4d). Because the syndrome in family 3 was named FH-II², we suggest using this term for patients with germline *CLCN2* variants.

Retrospectively, efforts to map the disease-causative gene in family 3³² were challenged by a phenocopy (sporadic idiopathic hyperaldosteronism) in subject 3-1, incomplete penetrance and phenotypic uncertainty. Rare *CLCN2* variants explained primary aldosteronism in ~10% of individuals in the early-onset cohort studied, suggesting that there are likely additional causative genes yet undiscovered. Genetic testing for germline mutations in *CLCN2* and other genes involved in early primary aldosteronism can be useful for establishing diagnosis, defining treatment options and assessing risk to future offspring.

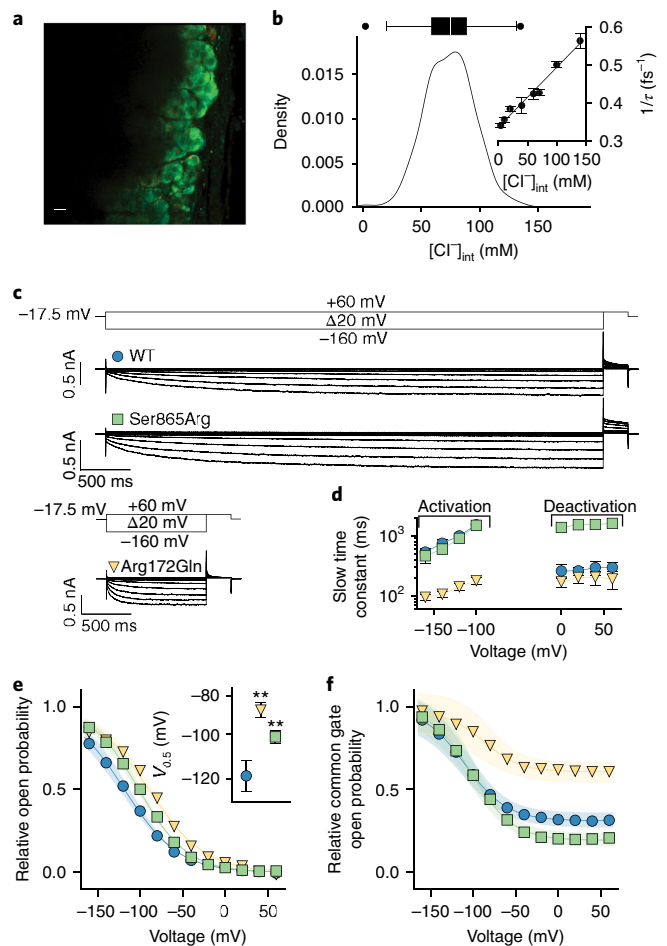


Fig. 3 | *CLCN2* mutations increase excitatory anion efflux by modifying the voltage dependence of channel opening.

a, Representative mouse adrenal gland section loaded with MQAE (1-(ethoxycarbonylmethyl)-6-methoxyquinolinium bromide) at 37 °C. Colors indicate high (short lifetimes, 1 ns; red) to low (long lifetimes, 4 ns; blue) intracellular chloride concentrations, with intermediate concentrations displayed in yellow to green shades (lifetimes of 2.5–3.5 ns). Scale bar, 10 μm . **b**, A kernel density estimation of intracellular chloride concentrations for glomerulosa cells was obtained (Gaussian kernel, bandwidth = 8.0 as determined by Scott's rule). The median intracellular chloride concentration was 74.7 mM (300 cells, 12 slices, five animals). Box, interquartile range; whiskers, 1.5 times the interquartile range; line, median. Inset, calibration curve of inverse MQAE fluorescence lifetimes ($1/\tau$) in cells with preset intracellular chloride concentrations. Data are shown as means \pm s.e.m. (233 cells, 6 slices, three mice). **c**, Whole-cell patch-clamp recordings of representative CIC-2^{WT} and CIC-2^{MUT} channels and the voltage protocol (150 mM $[\text{Cl}^-]_{\text{out}}$, 75 mM $[\text{Cl}^-]_{\text{int}}$; see the Methods for solutions; the number of cells is given in **e** and **f**). **d**, Time constants for representative CIC-2^{WT} and CIC-2^{MUT} channels. Data are shown as mean values with 95% confidence intervals (Supplementary Table 8). **e, f**, Mean relative open probabilities (**e**) and common gate open probabilities (**f**) were fit with a Boltzmann function (solid lines; Supplementary Table 8) with 95% confidence intervals as calculated from a bootstrap resampling (translucent areas). The open probabilities of mutant channels are significantly higher at the glomerulosa resting potential of about -80 mV (mean \pm s.e.m.: WT, 0.22 ± 0.02 ($n = 11$); p.Arg172Gln, 0.45 ± 0.02 ($n = 13$; $P < 0.001$ vs. WT); p.Ser865Arg, 0.33 ± 0.02 ($n = 12$; $P < 0.001$ vs. WT). The inset in **e** shows the shift in voltage activation as assessed by the point of half-maximal activation ($V_{0.5}$; data shown as means \pm s.e.m.; Supplementary Table 8). Statistical analysis was performed by one-way ANOVA ($F = 36.307$; degrees of freedom (d.f.) = 5): ** $P < 0.01$. Symbols are defined in **c**.

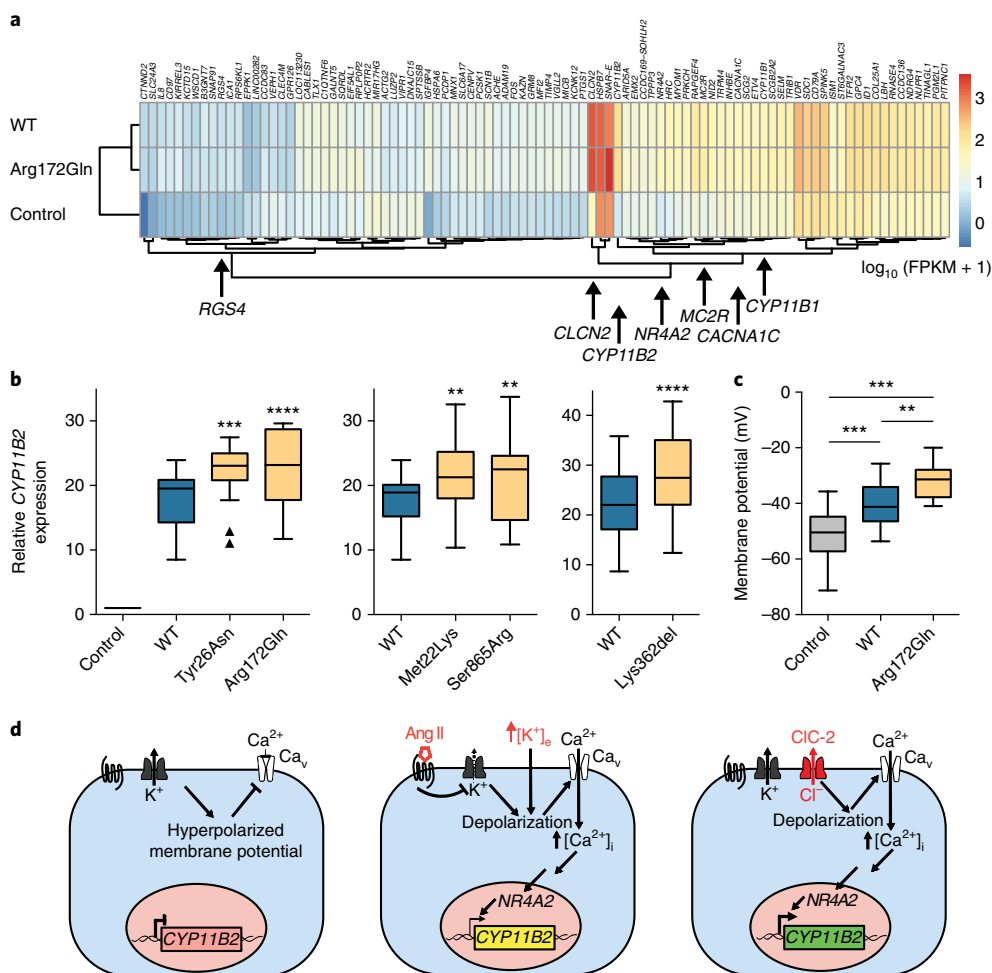


Fig. 4 | CIC-2 increases aldosterone synthase expression in H295R cells. a, RNA sequencing of H295R cells transfected with *CLCN2* (WT or Arg172Gln) or vector control. *CLCN2* and *CYP11B2* show the largest increase in expression versus control. Genes involved in adrenal function or calcium pathways are highlighted. FPKM, fragments per kilobase of transcript per million fragments mapped. **b**, Relative expression levels of *CYP11B2* (box, interquartile range; whiskers, 1.5 times the interquartile range; line, median) in the H295R cell line after transfection with empty vector (control), *CLCN2*^{WT} (blue) or *CLCN2*^{MUT} (orange). Parallel transfections and real-time PCR reactions were performed in each group. *CYP11B2* expression significantly increases after transfection with *CLCN2*^{MUT} (see Supplementary Table 8 for statistical analysis). **c**, Resting membrane potential (plots as in **b**) of HAC15 cells stably expressing *CLCN2* (WT or Arg172Gln) and untransfected controls. WT and Arg172Gln channels cause significant depolarization versus the control, and Arg172Gln causes significant depolarization versus WT channels (see Supplementary Table 8 for statistical analysis and tests used). **d**, Model of CIC-2 function in human adrenal glomerulosa. Resting cells are hyperpolarized. Ang II and hyperkalemia cause depolarization, activation of voltage-dependent calcium channels, calcium influx and increased *CYP11B2* expression via the transcription factor *NR4A2* (*NURR1*). *CIC-2*^{MUT} causes increased *CYP11B2* expression by membrane depolarization via increased chloride efflux. ***P* < 0.01; ****P* < 0.001; *****P* < 0.0001.

Proband with FH-II showed early-onset primary aldosteronism and hypertension, often with hypokalemia. Hypertension was controlled with mineralocorticoid receptor antagonists or other antihypertensives (Supplementary Note). This phenotype appears indistinguishable from that of patients with *CACNA1H* mutations¹³. Hybrid steroid production and/or response to glucocorticoids, historically used to diagnose GRA¹¹, was absent, as were massive adrenal hyperplasia (present in many subjects with *KCNJ5* variants^{6,12}) and neurodevelopmental abnormalities (characteristic of subjects with *CACNA1D* mutation⁷). Despite widespread *CLCN2* expression, subjects with gain-of-function *CLCN2* variants shared no apparent pathology other than primary aldosteronism, whereas loss-of-function *CLCN2* variants cause leukoencephalopathy with ataxia³³, with a similar phenotype in mice³⁴. Incomplete penetrance or phenotypic amelioration with age, as sometimes occurs with germline mutations in *CYP11B2*, *KCNJ5*, *CACNA1D* and *CACNA1H*^{7,12,13,35}, occurred in some subjects with *CLCN2* mutations.

Our findings implicate the activity of an anion channel in the regulation of aldosterone biosynthesis, primary aldosteronism and hypertension. Whether previously described slowly activating tiny chloride currents at strongly negative voltages in rat glomerulosa cells¹⁵ or Ras-dependent chloride currents³⁶ represent *CIC-2* activity is unclear. In vivo, *CIC-2* may contribute to hyperpolarization-induced depolarization of adrenal glomerulosa cells, cyclic membrane potential oscillations and aldosterone production²². Variants implicated in primary aldosteronism would likely amplify these effects. Mouse models may prove useful to study such effects.

Methods

Methods, including statements of data availability and any associated accession codes and references, are available at <https://doi.org/10.1038/s41588-018-0048-5>.

Received: 8 June 2017; Accepted: 20 December 2017;
Published online: 5 February 2018

References

- Monticone, S. et al. Prevalence and clinical manifestations of primary aldosteronism encountered in primary care practice. *J. Am. Coll. Cardiol.* **69**, 1811–1820 (2017).
- Stowasser, M. et al. Familial hyperaldosteronism type II: five families with a new variety of primary aldosteronism. *Clin. Exp. Pharmacol. Physiol.* **19**, 319–322 (1992).
- NCD Risk Factor Collaboration (NCD-RisC). Worldwide trends in blood pressure from 1975 to 2015: a pooled analysis of 1479 population-based measurement studies with 19.1 million participants. *Lancet* **389**, 37–55 (2017).
- Lim, S. S. et al. A comparative risk assessment of burden of disease and injury attributable to 67 risk factors and risk factor clusters in 21 regions, 1990–2010: a systematic analysis for the Global Burden of Disease Study 2010. *Lancet* **380**, 2224–2260 (2012).
- Funder, J. W. et al. The management of primary aldosteronism: case detection, diagnosis, and treatment: an Endocrine Society Clinical Practice Guideline. *J. Clin. Endocrinol. Metab.* **101**, 1889–1916 (2016).
- Choi, M. et al. K⁺ channel mutations in adrenal aldosterone-producing adenomas and hereditary hypertension. *Science* **331**, 768–772 (2011).
- Scholl, U. I. et al. Somatic and germline CACNA1D calcium channel mutations in aldosterone-producing adenomas and primary aldosteronism. *Nat. Genet.* **45**, 1050–1054 (2013).
- Azizan, E. A. et al. Somatic mutations in ATP1A1 and CACNA1D underlie a common subtype of adrenal hypertension. *Nat. Genet.* **45**, 1055–1060 (2013).
- Beuschlein, F. et al. Somatic mutations in ATP1A1 and ATP2B3 lead to aldosterone-producing adenomas and secondary hypertension. *Nat. Genet.* **45**, 440–444 (2013).
- Fernandes-Rosa, F. L. et al. Genetic spectrum and clinical correlates of somatic mutations in aldosterone-producing adenoma. *Hypertension* **64**, 354–361 (2014).
- Lifton, R. P. et al. A chimaeric 11 β -hydroxylase/aldosterone synthase gene causes glucocorticoid-remediable aldosteronism and human hypertension. *Nature* **355**, 262–265 (1992).
- Scholl, U. I. et al. Hypertension with or without adrenal hyperplasia due to different inherited mutations in the potassium channel KCNJ5. *Proc. Natl. Acad. Sci. USA* **109**, 2533–2538 (2012).
- Scholl, U. I. et al. Recurrent gain of function mutation in calcium channel CACNA1H causes early-onset hypertension with primary aldosteronism. *eLife* **4**, e06315 (2015).
- Korah, H. E. & Scholl, U. I. An update on familial hyperaldosteronism. *Horm. Metab. Res.* **47**, 941–946 (2015).
- Spät, A. & Hunyady, L. Control of aldosterone secretion: a model for convergence in cellular signaling pathways. *Physiol. Rev.* **84**, 489–539 (2004).
- Carss, K. J., Stowasser, M., Gordon, R. D. & O’Shaughnessy, K. M. Further study of chromosome 7p22 to identify the molecular basis of familial hyperaldosteronism type II. *J. Hum. Hypertens.* **25**, 560–564 (2011).
- Dong, C. et al. Comparison and integration of deleteriousness prediction methods for nonsynonymous SNVs in whole exome sequencing studies. *Hum. Mol. Genet.* **24**, 2125–2137 (2015).
- Genin, E., Tullio-Pelet, A., Begeot, F., Lyonnet, S. & Abel, L. Estimating the age of rare disease mutations: the example of Triple-A syndrome. *J. Med. Genet.* **41**, 445–449 (2004).
- Dogan, R. I., Getoor, L., Wilbur, W. J. & Mount, S. M. SplicePort—an interactive splice-site analysis tool. *Nucleic Acids Res.* **35**, W285–W291 (2007).
- Thiemann, A., Gründer, S., Pusch, M. & Jentsch, T. J. A chloride channel widely expressed in epithelial and non-epithelial cells. *Nature* **356**, 57–60 (1992).
- Untiet, V. et al. Glutamate transporter-associated anion channels adjust intracellular chloride concentrations during glial maturation. *Glia* **65**, 388–400 (2017).
- Hu, C., Rusin, C. G., Tan, Z., Guagliardo, N. A. & Barrett, P. Q. Zona glomerulosa cells of the mouse adrenal cortex are intrinsic electrical oscillators. *J. Clin. Invest.* **122**, 2046–2053 (2012).
- Jeworutzki, E. et al. GlialCAM, a protein defective in a leukodystrophy, serves as a Cl⁻ channel auxiliary subunit. *Neuron* **73**, 951–961 (2012).
- Stölting, G. et al. Regulation of ClC-2 gating by intracellular ATP. *Pflugers Arch.* **465**, 1423–1437 (2013).
- Niemeyer, M. I., Cid, L. P., Zúñiga, L., Catalán, M. & Sepúlveda, F. V. A conserved pore-lining glutamate as a voltage- and chloride-dependent gate in the ClC-2 chloride channel. *J. Physiol.* **553**, 873–879 (2003).
- Jentsch, T. J. Discovery of CLC transport proteins: cloning, structure, function and pathophysiology. *J. Physiol.* **593**, 4091–4109 (2015).
- Rainey, W. E., Bird, I. M. & Mason, J. I. The NCI-H295 cell line: a pluripotent model for human adrenocortical studies. *Mol. Cell. Endocrinol.* **100**, 45–50 (1994).
- Bassett, M. H., Suzuki, T., Sasano, H., White, P. C. & Rainey, W. E. The orphan nuclear receptors NURR1 and NGFIB regulate adrenal aldosterone production. *Mol. Endocrinol.* **18**, 279–290 (2004).
- Romero, D. G. et al. Regulators of G-protein signaling 4 in adrenal gland: localization, regulation, and role in aldosterone secretion. *J. Endocrinol.* **194**, 429–440 (2007).
- García-Olivares, J. et al. Gating of human ClC-2 chloride channels and regulation by carboxy-terminal domains. *J. Physiol.* **586**, 5325–5336 (2008).
- Tauber, P. et al. Cellular pathophysiology of an adrenal adenoma-associated mutant of the plasma membrane Ca²⁺-ATPase ATP2B3. *Endocrinology* **157**, 2489–2499 (2016).
- Lafferty, A. R. et al. A novel genetic locus for low renin hypertension: familial hyperaldosteronism type II maps to chromosome 7 (7p22). *J. Med. Genet.* **37**, 831–835 (2000).
- Depienne, C. et al. Brain white matter oedema due to ClC-2 chloride channel deficiency: an observational analytical study. *Lancet Neurol.* **12**, 659–668 (2013).
- Blanz, J. et al. Leukoencephalopathy upon disruption of the chloride channel ClC-2. *J. Neurosci.* **27**, 6581–6589 (2007).
- Stowasser, M. et al. Clinical, biochemical and genetic approaches to the detection of familial hyperaldosteronism type I. *J. Hypertens.* **13**, 1610–1613 (1995).
- Chorvátová, A., Gendron, L., Bilodeau, L., Gallo-Payet, N. & Payet, M. D. A Ras-dependent chloride current activated by adrenocorticotropin in rat adrenal zona glomerulosa cells. *Endocrinology* **141**, 684–692 (2000).

Acknowledgements

We thank our patients and their families for their invaluable contributions, the Yale Center for Genome Analysis for next-generation sequencing, the Center for Advanced Imaging (CAI) at Heinrich Heine University for providing a confocal microscope, S. Weidtkamp-Peters and S. Hänsch for technical assistance, J. Zhang for helpful discussions, E. Seidel, N. Erlenhardt and N. Klöcker for providing immunoprecipitation protocols and helpful discussions, C. Gomez-Sanchez (University of Mississippi) for providing plasmids, W. Rainey (University of Michigan) for providing HAC15 cells and M. Haase (Heinrich Heine University Düsseldorf) for providing H295R cells. Computational support and infrastructure were in part provided by the Centre for Information and Media Technology (Düsseldorf). This study was supported in part by the Ministerium für Kultur und Wissenschaft des Landes Nordrhein-Westfalen (Rückkehrprogramm and Junges Kolleg) and the Deutsche Forschungsgemeinschaft (SCHO 1386/2-1) (all to U.I.S.) and the NIH Center for Mendelian Genomics (5U54HG006504), NIH P01DK17433 and the Howard Hughes Medical Institute (all to R.P.L.).

Author contributions

U.I.S., G.S., C.F. and R.P.L. designed the study. M.S. and R.G. recruited and characterized family 3. A.M.O., C.G., D.M., R.W.L., D.P.J., G.C., P.G., E.L., C.N.-W. and R.P.L. ascertained and recruited probands with early-onset primary aldosteronism. A.A.V., E.L. and U.I.S. recruited additional members of selected families. C.N.-W., S.X. and A.W. prepared DNA samples. U.I.S., A.A.V., S.C.J., T.Y., M.C. and R.P.L. analyzed exome sequencing results. U.I.S. identified the disease-associated gene. C.N.-W., A.T. and A.A.V. performed and analyzed the results of targeted DNA sequencing. J.S. performed immunohistochemistry, immunoprecipitation and real-time PCR. J.S. and A.T. made constructs and generated stable cell lines. J.S. and J.C. prepared samples for and analyzed the results of RNA sequencing. J.S. and U.I.S. performed and analyzed the results of splicing assays and confocal microscopy. G.S., H.T., V.U. and C.F. performed and analyzed the results of FLIM and electrophysiology. M.K. and P.M. performed and analyzed the results of mass spectrometry. L.C.R. read and revised the manuscript. U.I.S. wrote the initial draft of the manuscript, with contributions and/or revisions from all authors.

Competing interests

Heinrich Heine University Düsseldorf has filed a patent application: EP17209972, Diagnosis and Therapy of Primary Aldosteronism.

Additional information

Supplementary information is available for this paper at <https://doi.org/10.1038/s41588-018-0048-5>.

Reprints and permissions information is available at www.nature.com/reprints.

Correspondence and requests for materials should be addressed to U.I.S.

Publisher’s note: Springer Nature remains neutral with regard to jurisdictional claims in published maps and institutional affiliations.

Methods

Subjects. Study subjects included the Australian kindred^{23,27}, 35 unrelated primary aldosteronism subjects without known disease-causing mutations, diagnosed by age 10 years (clinical characteristics published¹³), and 45 subjects diagnosed with primary aldosteronism by age 20 years (Supplementary Table 3). Selected families had additional members recruited. Controls were 3,578 unaffected parents of autistic offspring²⁸. Research protocols were approved by local institutional review boards at Yale University and the University of Queensland, and all probands and family members provided informed consent. Primary aldosteronism was diagnosed on the basis of elevated ARR (>20 ng/dl:ng/ml/h or equivalent values)⁵ with aldosterone >15 ng/dl or marginally elevated values in the presence of hypokalemia. Confirmatory testing was performed according to the referring centers' guidelines⁵. Venous blood or saliva samples were obtained from subjects and family members and subjected to exome and/or Sanger sequencing¹³.

DNA preparation and exome sequencing. DNA was prepared from venous blood or saliva samples using standard procedures. Exome capture was performed using the 2.1M NimbleGen Exome reagent (Roche NimbleGen), and 75-bp paired-end sequencing was performed on the Illumina platform with analysis performed as described¹³.

Sanger sequencing of genomic DNA and genotyping of parent-offspring trios. Direct bidirectional Sanger sequencing of candidate variants from genomic DNA of the indicated subjects was performed at Beckman Coulter Genomics or the Keck DNA sequencing facility at Yale University following PCR amplification. Rare variants identified in index cases through exome sequencing were genotyped by targeted PCR and Sanger sequencing in both parents to confirm paternity/maternity.

Immunohistochemistry and immunofluorescence. Formalin-fixed, paraffin-embedded 5- μ m human adrenal gland sections were obtained from US Biomax and Pantomics. Immunohistochemistry was performed as described⁷, with the exception that 10% donkey serum was used for blocking. The concentration of the antigenic peptide was 0.4 mg/ml, and 1 μ g of peptide per microgram of antibody was used. Images were recorded on a Zeiss AxioPlan 2 Imaging microscope (10 \times and 40 \times objectives) with a Zeiss AxioCam Mrc5 camera. Image cropping was performed in Adobe Illustrator CS4. The primary antibody against CIC-2 was HPA014545 (Sigma-Aldrich Prestige Antibodies; 1:100 dilution, incubation overnight at 4 $^{\circ}$ C), and the antibody against Dab2 was sc-13982 (Santa Cruz Biotechnology; 1:100 dilution). The secondary antibody was donkey anti-rabbit antibody (Jackson, 035-152, 1:200 dilution, incubation for 2 h at room temperature) for human samples. To confirm selection of the zona glomerulosa in mouse adrenal slices for FLIM, slices were stained with the antibody to Dab2 (1:100 dilution, incubation overnight at 4 $^{\circ}$ C). The secondary antibody was donkey anti-rabbit antibody conjugated to Alexa Fluor 647 (A-31573, Thermo Fisher Scientific, 1:1,000 dilution, incubation for 2 h at room temperature). Immunofluorescence images were recorded on a Leica TCS SP5 laser scanning confocal microscope (Leica Microsystems).

Molecular cloning. Site-directed mutagenesis (QuikChange, Agilent Technologies) was performed to introduce mutations into pcDNA5/FRT/TO CIC-2²⁴ according to the manufacturer's instructions. Primer sequences (M22K_F/_R, Y26N_F/_R, R172Q_F/_R, K362 del new_F/_R) are given in Supplementary Table 10. Each construct was validated by sequencing of the entire coding region. Mutant cDNAs were subcloned in frame into the pRcCMV vector containing YFP cDNA with NotI and PmlI for use in confocal microscopy only. Two independent clones were assessed in all experiments (Supplementary Fig. 3).

Generation of stable cell lines. Stable HEK293 cell lines were generated using the Flp-In T-REx system (Invitrogen, Life Technologies) according to the manufacturer's instructions. HEK293 cells do not express HEPACAM (Human Protein Atlas; see URLs). Flp-In T-REx 293 cells (authenticated, Eurofins Genomics) were cultured in high-glucose DMEM (Biochrom) with 10% FBS (Biochrom), 1% penicillin-streptomycin, 100 μ g/ml zeocin and 15 μ g/ml blasticidin (all Invitrogen) at 37 $^{\circ}$ C and 5% CO₂ in a humidified atmosphere. Cells were transfected with 2.4 μ g of pcDNA5/FRT/TO + insert (*CLCN2* mutants: p.Met22Lys, p.Tyr26Asn, p.Arg172Gln, p.Lys362del, p.Ser865Arg; two clones each) and 21.6 μ g of pOG44 using Lipofectamine 2000 (Invitrogen) and OptiMEM (Gibco by Life Technologies). The following day, the medium was changed to high-glucose DMEM supplemented with 10% Tet-free FBS (Gibco) and 1% penicillin-streptomycin. 48 h after transfection, cells were split onto 15-cm dishes and selected with 15 μ g/ml blasticidin and 150 μ g/ml hygromycin (Invitrogen). Single colonies were selected. Variants were confirmed by Sanger sequencing of DNA extracted from stable cell lines, and inducible expression was verified by western blot (CIC-2 antibody, ACL-002, Alomone Labs).

The HAC15 cell line was kindly provided by W. Rainey (University of Michigan), authenticated by short tandem repeat (STR) analysis (ATCC Cell Line Authentication Service) and cultured in DMEM/F12 (GlutaMAX, Gibco) supplemented with 5% HyClone Cosmic Calf Serum (CCS; GE Healthcare Life

Sciences), 1% penicillin-streptomycin (Gibco), 1% insulin transferrin selenium (ITS; Gibco), 1% MEM Non-Essential Amino Acids Solution (Gibco) and 0.1% CD Lipid Concentrate (Gibco) at 37 $^{\circ}$ C and 5% CO₂ in a humidified atmosphere. Stable cell lines were prepared using the Piggybac transposon system (System Biosciences). cDNAs of *CLCN2* (wild type and encoding p.Arg172Gln) were subcloned into pENTR-2B-Dual using NotI and XhoI. Gateway LR recombination (Invitrogen) was performed with pPiggybac-EF1 Neo and pTF rTA (a kind gift of C. Gomez-Sanchez, University of Mississippi). Inserts were verified by Sanger sequencing. HAC15 cells were transfected using an Amaxa Nucleofector I (Lonza; 2 million cells, 2 μ g of plasmid DNA, 0.8 μ g of Super Piggybac transposase; program X-005). After 48 h, selection was initiated by addition of 5 μ g/ml blasticidin (Gibco) to the growth medium. Inducible expression was verified by western blot (CIC-2 antibody, ACL-002) after incubation with 1 μ g/ml doxycycline (Sigma-Aldrich) for 24 h.

Preparation of acute adrenal slices. After anesthetizing mice with isoflurane and decapitation, both adrenal glands were rapidly removed and placed in ice-cold bicarbonate-buffered saline (BBS) (125 mM NaCl, 2 mM KCl, 26 mM NaHCO₃, 0.1 mM CaCl₂, 5 mM MgCl₂, 10 mM glucose, constantly oxygenated with 5% CO₂ in O₂) for the removal of surrounding fat. The adrenal glands were embedded in 4% agarose in BBS, mounted, cut at 4 $^{\circ}$ C (150–200 μ m thick) with a Microm HM 650V (Thermo Scientific; frequency 60 Hz, amplitude 1 mm, drive 10) and held at 35 $^{\circ}$ C for 30 min in BBS. Slices were subsequently stored in BBS at 37 $^{\circ}$ C for further experiments. During each experiment, slices were constantly perfused with solution at 37 $^{\circ}$ C, and all measurements were completed within 8 h of organ removal.

Fluorescence lifetime imaging microscopy. Prior to chloride imaging experiments, adrenal slices were incubated in BBS containing 10 mM MQAE (Sigma-Aldrich)³⁹ for 45–60 min at room temperature. Slices were transferred to an imaging chamber and perfused with BBS solution containing 2 mM instead of 0.1 mM Ca²⁺; FLIM was performed as described²¹. The solution was perfused through a heating coil, resulting in a temperature of 37 $^{\circ}$ C in the perfusion chamber. Fluorescence was stimulated by two-photon excitation (λ_{exc} = 750 nm). MQAE fluorescence was filtered (short-pass filter 500 nm, λ_{obs} < 510 nm; Omega Optical), and mean fluorescence lifetimes were measured using multidimensional time-correlated single-photon counting (TCSPC). TCSPC electronics (SPC-152, Becker & Hickl) and acquisition software were used for FLIM as described⁴⁰. We recorded data for 12 slices from five different C57BL/6 mice (two male, three female) of age 3 months or older.

For chloride concentration calibration, MQAE fluorescence lifetimes of preset [Cl⁻] values were measured. Adrenal slices were incubated in HEPES-buffered solution (140 mM K⁺, 10 mM Na⁺, 10 mM HEPES, 10–80 mM Cl⁻, 70–140 mM gluconate, adjusted to 310 mOsm/L with potassium gluconate and to pH 7.4 with KOH, 37 $^{\circ}$ C) containing 10 μ M nigericin (sodium salt; Sigma-Aldrich) and 10 μ M tributyltin (chloride salt; Sigma-Aldrich)^{21,40–42}. The inverse fluorescence lifetime (1/ τ) was plotted, and the calibration curve was fitted as described before²¹. The Stern–Volmer constant (K_{SV} = 3.96) was determined as the product of τ_0 and the slope of the calibration curve. Because the fluorescence lifetime of MQAE is reduced by chloride via collisional quenching, MQAE fluorescence lifetimes and [Cl⁻] show a linear relationship.

$$\frac{\tau_0}{\tau} = 1 + K_{SV}[\text{Cl}^-]$$

Zona glomerulosa [Cl⁻]_{int} could then be calculated according to this relationship.

The three outermost cell layers were assumed to form the zona glomerulosa based on their characteristic nucleus-to-cytoplasm ratio and the corresponding staining with antibody to DAB2 (sc-13982, Santa Cruz Biotechnology) performed separately. Each cell was defined as a region of interest (ROI) with the exclusion of the nucleus, and fluorescence lifetimes were determined as mean values of the average fluorescence lifetimes of all pixels in a given ROI. Fluorescence lifetimes were calculated using SPCImage 5.6 (Becker & Hickl) and exported for further extraction in Fiji. Statistical analysis was performed using SigmaPlot 12 (Systat) and Python 3.5.2 + numpy 1.12.1 + scipy 0.18.1 + pandas 0.19.2 + seaborn 0.7.1 using built-in functions. The FLIM datasets generated or analyzed during the current study are available on request. Python scripts for analysis are based on built-in functions of the above-mentioned packages but are available on request.

Electrophysiological recordings. Flp-In T-REx stable cell lines were used for electrophysiological recordings. For each construct, at least two clones from at least two separate preparations were included in the analysis. To avoid chloride depletion at large current amplitudes²⁴, Flp-In T-REx cells were used without induction. Whole-cell patch-clamp currents were recorded on an EPC10 amplifier using PatchMaster software (both HEKA). Borosilicate glass pipettes with open resistances between 0.9 and 2.5 M Ω were used. The extracellular solution for whole-cell recordings contained (in mM) 140 NaCl, 4 KCl, 2 CaCl₂, 1 MgCl₂, and 10 HEPES at pH 7.4. The intracellular solution contained (in mM) 73 NaCl, 1 MgCl₂, 42 sodium gluconate, 5 EGTA, 10 HEPES and 1 Mg-ATP at pH 7.4. The liquid

junction potential was calculated to be 1.9 mV and corrected for a priori. Cells were held at the calculated chloride reversal potential of -17.5 mV at rest.

Instantaneous current amplitudes at the fixed tail step to +60 mV were normalized and plotted against the preceding voltage step to show relative open probability curves. The durations of the voltage steps were 5 s for CLC-2^{WT} and CLC-2^{Ser865Arg} and 1 s for all other mutants, so that steady-state open probabilities were determined. Open probabilities (P_{open}) were fitted using a modified Boltzmann equation

$$P_{open}(V) = \frac{1}{1 + e^{-\frac{V - V_{1/2}}{k}}}$$

to allow for a comparison of the half-maximal activation ($V_{1/2}$).

Fitting of the activation and deactivation current traces with the sum of two exponential functions revealed fast (τ_f) and slow (τ_s) time constants, respectively.

$$I(t) = A_0 + A_1 \cdot e^{-\frac{t}{\tau_f}} + A_2 \cdot e^{-\frac{t}{\tau_s}}$$

CLC chloride channels are double-barreled channels with two conduction pathways. Protopores can be individually opened and closed by a fast gating process, but also jointly by slow common gating. Under the assumption that protopore and common gating processes are independent, the overall open probability equals the product of the respective individual open probabilities⁴⁵.

$$P_{open} = P_{fast} \cdot P_{slow}$$

By inserting a 15-ms pulse to -220 mV between the variable test pulse and the tail pulse, the CLC-2 fast gate is maximally opened ($P_{fast} = 1$)⁴⁴, and the common gate open probability can be determined. Fast protopore gate open probabilities were calculated by dividing the overall open probability by the common gate open probability.

Resting potentials in untransfected or induced (1 μ g tetracycline/ml medium for 24 h) stably transfected HAC15 cells were measured using the perforated patch technique⁴⁵ in the current-clamp mode. The extracellular solution contained (in mM) 140 NaCl, 10 HEPES, 4 KCl, 2 CaCl₂ and 1 MgCl₂ adjusted to a pH of 7.4. The pipette solution contained (in mM) 130 KCl, 10 HEPES and 5 NaCl with the pH adjusted to 7.4. To maintain the native intracellular [Cl⁻], we included the pore-forming, monovalent-cation-selective antibiotic gramicidin D (Sigma-Aldrich) in the pipette solution to obtain access to the inside of the cell⁴⁵. Gramicidin stock solution (50 mg/ml in DMSO) was prepared daily, and the diluted solution (final concentration of 100 μ g/ml) was prepared every 2 h. The tip of the pipette (open resistance of 1.5–3 M Ω) was filled with solution lacking gramicidin to facilitate gigaseal formation. Break-in was typically observed after 15–45 min. Resting potentials were determined using a HEKA EPC-10 patch-clamp amplifier and PatchMaster software (HEKA Elektronik) from the mean of 10- to 60-s voltage recording segments with the current clamped to 0 pA. Only cells that exhibited CLC-2-like currents (visible slow activation upon hyperpolarization and a current larger than 40 pA at -160 mV in subsequent voltage-clamp experiments) were used for analysis.

Analysis of all electrophysiological experiments was performed using FitMaster software (HEKA Elektronik), SigmaPlot 12 (Systat) and Python 3.5.2 + numpy 1.12.1 + scipy 0.18.1 + pandas 0.19.2 using built-in functions. The electrophysiology datasets generated or analyzed during the current study are available on request. Python scripts for analysis are based on built-in functions of the above-mentioned packages but are available on request. Normality was assessed by Shapiro–Wilk test.

Culture of H295R cells. H295R human adrenocortical cells (a kind gift of M. Haase, Heinrich Heine University) were authenticated by STR analysis (ATCC Cell Line Authentication Service) and cultured in DMEM/F12 supplemented with HEPES (Gibco), 2.5% Ultrosor G (Pall), 1% ITS (Corning) and 1% penicillin-streptomycin (Gibco) at 37 °C and 5% CO₂ in a humidified atmosphere.

Quantitative real-time PCR. Three million H295R cells were resuspended in 100 μ l of Nucleofector solution R (Lonza) plus 3 μ g of plasmid DNA (pcDNA/FRT/TO empty vector, wild-type or mutant *CLCN2*) and electroporated with program P-20 using an Amaxa Nucleofector I (Lonza). After recovering the cells in RPMI-1640 medium (Gibco) for 15 min at 37 °C, cells were plated on 12-well plates. 24 h after transfection, H295R cells were starved in DMEM/F12 supplemented with HEPES, 0.1% Ultrosor G and 1% penicillin-streptomycin for an additional 24 h. Total RNA was isolated using the RNeasy Mini kit (Qiagen) and quantified with a Nanodrop 2000 (Thermo Scientific). After reverse transcription of RNA using the QuantiTect reverse transcription kit (Qiagen), TaqMan gene expression assays (Applied Biosystems) for *GAPDH* (Hs02758991_g1) as a housekeeping gene and *CYP11B2* (Hs01597732_m1) as the gene of interest were performed using TaqMan Gene Expression Master Mix. Each variant was assessed in parallel with empty vector control or vector expressing wild type. Gene expression was evaluated relative to the housekeeping gene and expressed as 2 ^{$\Delta\Delta C_t$} . Normality was assessed by Shapiro–Wilk test. Statistical differences were assessed by ratio-paired two-tailed *t* tests

(for normally distributed individual data), one-way ANOVA (for normally distributed multiple comparisons; adjusted *P* value reported) or Friedman test (multiple comparisons, no normal distribution; adjusted *P* value reported) in GraphPad Prism 7.

Whole-transcriptome sequencing, read alignment and differential gene expression analysis. H295R cells were transfected in two independent reactions as above, and RNA was isolated using TRIzol (Thermo Fisher Scientific) followed by DNase digestion and column purification (RNeasy, Qiagen). Libraries were prepared after poly(A) selection. Samples were sequenced on the Illumina HiSeq 2500 instrument at the Yale Center for Genome Analysis, producing a mean of 47.9 million 75-bp single-end reads. The quality of the raw sequencing reads was evaluated using FastQC version 0.10.4 (see URLs), and the base of lower quality (base quality score < 20) in the last position was trimmed. TopHat v2.1.1⁴⁶ was used to align the high-quality sequencing reads to reference human genome sequence build hg19. Differentially expressed genes were identified by Cuffdiff v2.2.1⁴⁷. An FDR-adjusted *P* value (*q* value) ≤ 0.05 and $|\log_2(\text{fold change})| \geq 1$ were set as the cutoffs for significant differential expression.

Estimation of the probability of observing one de novo and two transmitted p.Arg172Gln variants in CLCN2. From the identification of the novel p.Arg172Gln variant in family 3, we calculated the probability of finding an identical de novo mutation and two independent instances of the same transmitted variant by chance among 80 probands. Using the genome-wide mutation rate of 1.67×10^{-8} mutations per base per generation from a recent study⁴⁸, we estimated that the probability of seeing any specific de novo mutation in one individual is 3.34×10^{-8} . For transmitted events, we applied the UnseenEst⁴⁹ algorithm to estimate the probability of finding an unseen missense mutation in human populations. A total of 33,778 healthy individuals were selected from the ExAC database⁵⁰ to match the population distribution of the 2010 US Census. The US Census-matched dataset was trained in the UnseenEst⁴⁹ algorithm to estimate the frequency distribution of distinct unseen missense mutations for the US population. The predicted frequency distribution was used to extrapolate the probability of observing one unseen transmitted event (probability = 2.81×10^{-5}). Taken together, the probability of observing one de novo and two transmitted p.Arg172Gln variants among 80 independent samples is estimated as follows.

$$\binom{80}{2} \times (2.81 \times 10^{-5})^2 \times (1 - 2.81 \times 10^{-5})^{78} \times \binom{78}{1} \times (3.34 \times 10^{-8})^1 \times (1 - 3.34 \times 10^{-8})^{77} = 6.49 \times 10^{-12}$$

Shared haplotypes and estimation of the age of the mutation encoding p.Arg172Gln in CLCN2. Genotypes of SNPs flanking the *CLCN2*^{Arg172Gln} mutation were extracted from exome data. To estimate the age of the mutation in *CLCN2* encoding p.Arg172Gln testing the assumption that the mutation is identical by descent among each possible pair of kindreds with the variant (except the documented de novo mutation), we used the ESTIAGE algorithm to estimate the pairwise time of coalescence for the three pairs of kindreds as previously described^{13,18}. ESTIAGE uses a maximum-likelihood approach to estimate the mutation age, which takes into account the frequencies of the shared allele at each marker and the recombination fractions between the mutation of interest and polymorphic markers located within or at the boundaries of the shared haplotype. Seventeen polymorphic markers spanning the shared haplotype were used for input (Supplementary Table 5). The marker allele frequencies were estimated from the Finnish and non-Finnish European populations in the ExAC database⁵⁰, and the mutation rate was set to 2×10^{-8} .

Statistics. The statistical analyses used throughout the manuscript are described in the corresponding results and methods paragraphs, figure legends or supplementary tables.

URLs. ClinVar, <https://www.ncbi.nlm.nih.gov/clinvar/>; HEPACAM localization in Human Protein Atlas (retrieved 27 June 2017), <http://www.proteinatlas.org/ENSG00000165478-HEPACAM/cell/HEK+293>; FastQC, <https://www.bioinformatics.babraham.ac.uk/projects/fastqc/>; GTEx Portal HEPACAM expression, <http://www.gtexportal.org/home/gene/HEPACAM>.

Life Sciences Reporting Summary. Further information on experimental design is available in the Life Sciences Reporting Summary.

Code availability. Code for gene burden analysis is available at GitHub (https://github.com/murim76/gene_burden_test/blob/master/Compare_VCF_for_Scholl.pl).

Data availability. *CLCN2* variants have been deposited in ClinVar (accessions 441164, 441165, 441166, 441167 and 441168), and RNA-seq data have been deposited at GEO (accession GSE107030).

References

37. Torpy, D. J. et al. Familial hyperaldosteronism type II: description of a large kindred and exclusion of the aldosterone synthase (*CYP11B2*) gene. *J. Clin. Endocrinol. Metab.* **83**, 3214–3218 (1998).
38. Krumm, N. et al. Excess of rare, inherited truncating mutations in autism. *Nat. Genet.* **47**, 582–588 (2015).
39. Verkman, A. S. Development and biological applications of chloride-sensitive fluorescent indicators. *Am. J. Physiol.* **259**, C375–C388 (1990).
40. Kaneko, H., Putzier, L., Frings, S., Kaupp, U. B. & Gensch, T. Chloride accumulation in mammalian olfactory sensory neurons. *J. Neurosci.* **24**, 7931–7938 (2004).
41. Bevensee, M. O., Apkon, M. & Boron, W. F. Intracellular pH regulation in cultured astrocytes from rat hippocampus. II. Electrogenic Na/HCO₃ cotransport. *J. Gen. Physiol.* **110**, 467–483 (1997).
42. Chao, A. C., Dix, J. A., Sellers, M. C. & Verkman, A. S. Fluorescence measurement of chloride transport in monolayer cultured cells. Mechanisms of chloride transport in fibroblasts. *Biophys. J.* **56**, 1071–1081 (1989).
43. Accardi, A. & Pusch, M. Fast and slow gating relaxations in the muscle chloride channel CLC-1. *J. Gen. Physiol.* **116**, 433–444 (2000).
44. de Santiago, J. A., Nehrke, K. & Arreola, J. Quantitative analysis of the voltage-dependent gating of mouse parotid ClC-2 chloride channel. *J. Gen. Physiol.* **126**, 591–603 (2005).
45. Rhee, J. S., Ebihara, S. & Akaike, N. Gramicidin perforated patch-clamp technique reveals glycine-gated outward chloride current in dissociated nucleus solitarii neurons of the rat. *J. Neurophysiol.* **72**, 1103–1108 (1994).
46. Kim, D. et al. TopHat2: accurate alignment of transcriptomes in the presence of insertions, deletions and gene fusions. *Genome Biol.* **14**, R36 (2013).
47. Trapnell, C. et al. Differential analysis of gene regulation at transcript resolution with RNA-seq. *Nat. Biotechnol.* **31**, 46–53 (2013).
48. Samocha, K. E. et al. A framework for the interpretation of de novo mutation in human disease. *Nat. Genet.* **46**, 944–950 (2014).
49. Zou, J. et al. Quantifying unobserved protein-coding variants in human populations provides a roadmap for large-scale sequencing projects. *Nat. Commun.* **7**, 13293 (2016).
50. Lek, M. et al. Analysis of protein-coding genetic variation in 60,706 humans. *Nature* **536**, 285–291 (2016).

Life Sciences Reporting Summary

Nature Research wishes to improve the reproducibility of the work that we publish. This form is intended for publication with all accepted life science papers and provides structure for consistency and transparency in reporting. Every life science submission will use this form; some list items might not apply to an individual manuscript, but all fields must be completed for clarity.

For further information on the points included in this form, see [Reporting Life Sciences Research](#). For further information on Nature Research policies, including our [data availability policy](#), see [Authors & Referees](#) and the [Editorial Policy Checklist](#).

▶ Experimental design

1. Sample size

Describe how sample size was determined.

Sample sizes for electrophysiological recordings and FLIM experiments were estimated according to previous experience with similar proteins and experimental setups; sample size for real-time PCRs was estimated based on electrophysiological results and results of RNAseq.

2. Data exclusions

Describe any data exclusions.

For electrophysiological recordings (technically acceptable recording, presence of CIC-2-like currents) and FLIM (outer layers of the adrenal gland as described in Methods) experiments, only inclusion criteria were defined with no data being excluded afterwards.
For CYP11B2 qPCR (Figure 4C), the first transfection was excluded because the experimentator performed this protocol and transfection (via electroporation) for the first time and used it for practice.
For confocal microscopy, cells without sufficient detection of CFP and/or YFP were excluded.
For membrane potential measurements, cells without CIC-2-like currents were excluded.

3. Replication

Describe whether the experimental findings were reliably reproduced.

Electrophysiological experiments, FLIM data, real-time PCRs, and confocal microscopy were performed using multiple separate preparations and at least two DNA or stable cell line clones and were reliably reproduced. IHC was reliably reproduced (2 technical replicates each of two biological replicates). Splicing assay was performed using two independent clones with indistinguishable results. Mass spectrometry was performed on two independent preparations, with reproducible results. Similar results were obtained from two preparations using a different solvent.

4. Randomization

Describe how samples/organisms/participants were allocated into experimental groups.

Samples for electrophysiological, FLIM experiments, confocal microscopy, IHC and real-time PCRs were not randomized.

5. Blinding

Describe whether the investigators were blinded to group allocation during data collection and/or analysis.

For electrophysiological, FLIM and RNA sequencing experiments, investigators were not blinded to group allocation. For CYP11B2 qPCR (Figure 4C) the investigator was blinded to group allocation of two replicates by replacing the plasmid names with numbers.
The investigator was not blinded to group allocation for confocal microscopy and immunohistochemistry.

Note: all studies involving animals and/or human research participants must disclose whether blinding and randomization were used.

6. Statistical parameters

For all figures and tables that use statistical methods, confirm that the following items are present in relevant figure legends (or in the Methods section if additional space is needed).

- n/a | Confirmed
- The exact sample size (n) for each experimental group/condition, given as a discrete number and unit of measurement (animals, litters, cultures, etc.)
 - A description of how samples were collected, noting whether measurements were taken from distinct samples or whether the same sample was measured repeatedly
 - A statement indicating how many times each experiment was replicated
 - The statistical test(s) used and whether they are one- or two-sided (note: only common tests should be described solely by name; more complex techniques should be described in the Methods section)
 - A description of any assumptions or corrections, such as an adjustment for multiple comparisons
 - The test results (e.g. P values) given as exact values whenever possible and with confidence intervals noted
 - A clear description of statistics including central tendency (e.g. median, mean) and variation (e.g. standard deviation, interquartile range)
 - Clearly defined error bars

See the web collection on [statistics for biologists](#) for further resources and guidance.

► Software

Policy information about [availability of computer code](#)

7. Software

Describe the software used to analyze the data in this study.

Analysis of all electrophysiological experiments were performed using FitMaster software (HEKA Elektronik), SigmaPlot 12 (Systat) and Python 3.5.2+numpy 1.12.1+scipy 0.18.1+pandas 0.19.2 using built-in functions. Fluorescence lifetimes were calculated using SPCLImage 5.6 (Becker&Hickl) and exported for further extraction in Fiji. Statistics were performed using SigmaPlot 12 (Systat) and Python 3.5.2+numpy 1.12.1+scipy 0.18.1+pandas 0.19.2+seaborn 0.7.1 using built-in functions. Real-time PCR results were analyzed with Microsoft Excel 2010 and Graph Pad Prism 6. Confocal microscopy was analyzed in ZEN 2012 (black edition, Carl Zeiss) and Graphpad Prism 6. Mass spectrometry was analyzed using MaxQuant version 1.5.1.2.

For manuscripts utilizing custom algorithms or software that are central to the paper but not yet described in the published literature, software must be made available to editors and reviewers upon request. We strongly encourage code deposition in a community repository (e.g. GitHub). [Nature Methods guidance for providing algorithms and software for publication](#) provides further information on this topic.

► Materials and reagents

Policy information about [availability of materials](#)

8. Materials availability

Indicate whether there are restrictions on availability of unique materials or if these materials are only available for distribution by a for-profit company.

There are restrictions on availability of subject DNAs and exome sequencing data because of a lack of consent for data sharing and potential identification of subjects from exome data.

9. Antibodies

Describe the antibodies used and how they were validated for use in the system under study (i.e. assay and species).

Anti-CLCN2 (HPA014545): Sigma-Aldrich; Lot # R06751; polyclonal; IgG; validation is described in human protein atlas (<http://www.proteinatlas.org/ENSG00000114859-CLCN2/antibody>)
 Dab2 (H-110): Santa Cruz sc-13982; Lot # E3013; polyclonal; validation is described in the following citations: PMID: # 24889971, PMID: # 23293299, PMID: # 23840954

10. Eukaryotic cell lines

a. State the source of each eukaryotic cell line used.

H295R: gift of Dr. Matthias Haase (HHU Düsseldorf); HAC15: gift of Dr. William Rainey (University of Michigan); Flp-In-T-REx 293 cells were obtained from Invitrogen.

b. Describe the method of cell line authentication used.

H295R/HAC15: short tandem repeat (STR) analysis by ATCC (03/30/2016)
HEK293T: short tandem repeat (STR) analysis by Eurofins Genomics (10/13/2016)

c. Report whether the cell lines were tested for mycoplasma contamination.

H295R, HAC15 and HEK293 tested negative for mycoplasma contamination.

d. If any of the cell lines used are listed in the database of commonly misidentified cell lines maintained by [ICLAC](#), provide a scientific rationale for their use.

H295R and HAC15 (as a subclone of H295R) are the most established human aldosterone-producing adrenal cell lines. We used HAC15 for stable cell line generation because H295R is not a clonal cell line. HEK293 cells are an established system for patch clamp electrophysiology.

► Animals and human research participants

Policy information about [studies involving animals](#); when reporting animal research, follow the [ARRIVE guidelines](#)

11. Description of research animals

Provide details on animals and/or animal-derived materials used in the study.

Five CL57BL/6 mice were used for FLIM experiments (2 males, 3 females, age > 3mo)

Policy information about [studies involving human research participants](#)

12. Description of human research participants

Describe the covariate-relevant population characteristics of the human research participants.

This information is provided in Table 1 and Supplementary Table 3 of the manuscript. Additional probands are described in Ref. 13.